Mechanofluorochromism of pyrene-derived amidophosphonates

Yuichi Hirai, Anna Wrona- Piotrowicz, Janusz Zakrzewski, Arnaud Brosseau, Régis Guillot, Rémi Métivier, Clémence Allain

ARTICLE

Mechanofluorochromism of Pyrene–Derived Amidophosphonates

Yuichi Hirai,[a] Anna Wrona-Piotrowicz,[b] Janusz Zakrzewski,[b] Arnaud Brosseau,[a] Régis Guillot,[c] Rémi Métivier*[a] and Clémence Allain*[a]

Received 00th January 20xx,
Accepted 00th January 20xx

DOI: 10.1039/x0xx00000x

Aiming to develop a library of organic mechanofluorochromic (MFC) materials, solid-state emission properties of pyrene-derivatives with amidophosphonate groups (diethyl 1-(pyrene-1-carboxamido)alkylphosphonates, alkyl: methyl, isopropyl, phenyl) were investigated. All of these compounds were found to show strong blue fluorescence, and blue-to-green emission shift was identified upon grinding. Monomer and several excimer emissive species were identified by steady-state and time-resolved fluorescence investigations. The characteristic green-to-blue thermal back reaction was observed even at room temperature without additives, which would be related to the flexibility of side groups for molecular rearrangement. We here demonstrated that the pyrene-derived compounds can be attractive platforms to host MFC properties.

Introduction

Mechanofluorochromism (MFC) refers to reversible change in fluorescence emission wavelength of solid-state materials upon mechanical stimuli, and has emerged as a new optical function of luminescent materials in the last decade.[1, 2] Mechanical grinding and shearing of fluorescent molecules have been reported to trigger crystal-to-crystal phase change or crystal-to-amorphous structural deformation, resulting in molecular-arrangement alteration to exhibit different optoelectronic properties. MFC behaviours have been identified for organic, organometallic, and polymer compounds.[3-5] A series of boron *б*-diketonates and gold(I)-isocyanides are well-known MFC candidates due to their excimer formation and metal-to-metal distance alteration.[6-9] A combination of rigid axes/planes and mobile side groups has enabled the modification of these supramolecular arrangements upon mechanical stimulation.

Herein, we focused on pyrene-derived compounds due to the planar and fluorescent pyrene moiety and synthetic diversity of side groups. Pyrene derivatives have been investigated extensively for their strong fluorescence in solution[10-12] and in the solid state.[13] Recently, a series of solid-state strong fluorescent pyrenes were reported for the formation of face-to-face or edge-to-face stacking depending on the number of acetyl groups.[14] The different molecular arrangement of pyrenes also induced a wide variety of fluorescence emission colour from blue to yellow. The fluorescence and π-aromatic-based variable packing structures can accommodate mechanical-force sensitivity, and in the literature pyrene derivatives substituted with amides,[15, 16] boronic acids or esters,[17] phosphonium groups[18] or more sophisticated dendritic structures[19] displaying MFC properties have been described. These examples show that investigation of a wide variety of pyrene derivatives is important to introduce a new library of MFC-active compounds. Alteration of small side groups can be very interesting to see the effect on MFC properties. In terms of synthetic diversity, amido substituted pyrenes are promising candidates because of their versatile synthesis: they can be obtained either from pyrene-1-carboxylic acid or by reacting pyrene with isothiocyanates, then desulfurizing the pyrene-1-carbothioamide intermediate, as reported by some of us.[10]

We previously reported the strong fluorescence properties of pyrene amidophosphonates in solution (figure 1 top, quantum yields Φ = 63-68% in chloroform),[20] and showed that phosphonate groups have significant influence on the excited state deactivation scheme, increasing the radiative pathway (k_r) and decreasing the non-radiative one (k_{nr}) compared to simpler amide analogues. These classes of derivatives were identified as promising solid-state emitters.

[a] Université Paris-Saclay, ENS Paris-Saclay, CNRS, PPSM, 94235 Cachan, France. Emails : remi.metivier@ens-paris-saclay.fr, clemence.allain@ens-paris-saclay.fr
[b] Department of Organic Chemistry, Faculty of Chemistry, University of Łódź, Tamka 12, 91-403 Łódź, Poland.
[c] Université Paris-Saclay, CNRS, ICMMO, 91405 Orsay, France.

Electronic Supplementary Information (ESI) available: [spectroscopic data in solution and in the solid state]. See DOI: 10.1039/x0xx00000x

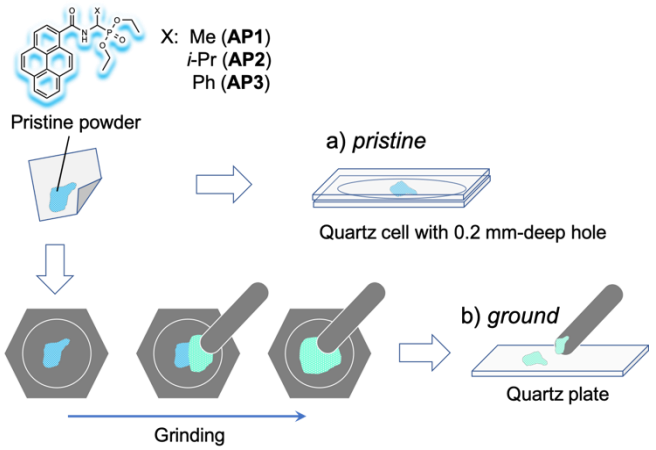

Figure 1. Sample preparation of a) pristine and b) ground pyrene-derived amidophosphonates (**AP1-3**) for spectroscopy.

Results and discussion

Diethyl 1-(pyrene-1-carboxamido)alkylphosphonates **AP1-3** were synthesized following our previously published procedure.[20] Slow evaporation of dichloromethane/ethanol solution yielded the single crystals of **AP1-3** in space groups $P2_1/c$, $C2/c$ and $P\text{-}1$, respectively (Figure 2, see Table S1 for crystallographic parameters). The crystal packing structures of **AP1-3** are similar to that of hydrogen-substituted amidophosphonate (denoted "**AP-H**" hereafter)[20] with shifted face-to-face π-π stacking (Figure 2 right, $d_{\pi\text{-}\pi}$ = 3.43, 3.37, 3.38 Å for **AP1-3**, respectively). A pair of π-π stacked pyrene units of **AP2** forms additional CH-π interactions ($d_{CH\text{-}\pi}$ = 2.61 Å, $\angle_{CH\text{-}\pi}$ = 88˚) with another pair. The pyrene units of **AP3** form a columnar stacking structure along the direction of a-axis, and the phenyl side groups are also involved in forming CH-π interactions ($d_{CH\text{-}\pi}$ = 2.40 Å, $\angle_{CH\text{-}\pi}$ = 89˚), while **AP1** does not exhibit these strong edge-to-face contacts.

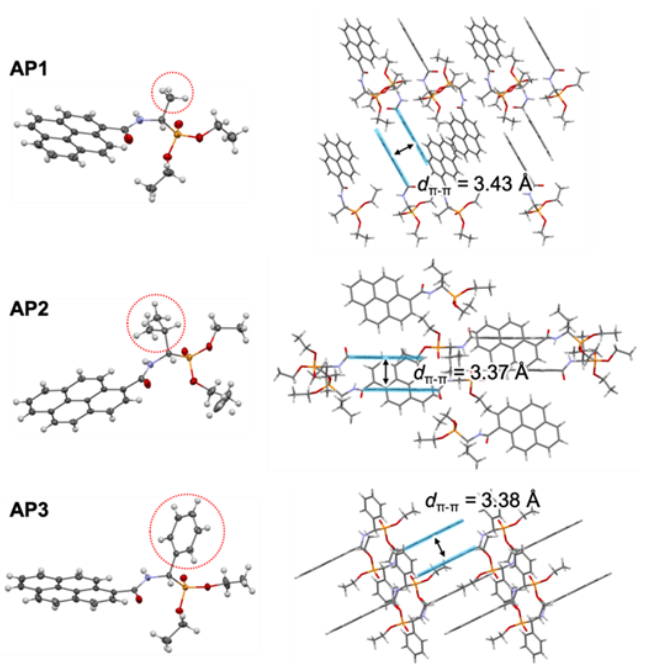

Figure 2. ORTEP drawings of single molecules (left) and packing structures (right) of **AP1-3**. Thermal ellipsoids are shown at the 30% level.

Electronic absorption and emission spectra of **AP1-3** in 10^{-6} M chloroform solution are shown in Figure S1 in supporting information. The nearly identical structured emission bands, with maxima at 385-387 nm, show a slight effect of side groups in solution. The time-resolved fluorescence study also reveals the quite similar emission lifetimes in the range of 9-11 ns (see supporting information Table S2). We here attempted to investigate the MFC properties of these series of compounds. In order to compare the pristine and ground forms, we prepared samples of both forms for spectroscopy (Figure 1). A quartz cell with 0.2 mm-deep hole was used for pristine state in order not to apply mechanical stimulation. After grinding the powder, a quartz plate was directly scratched with a pestle for spectroscopy of the ground materials.

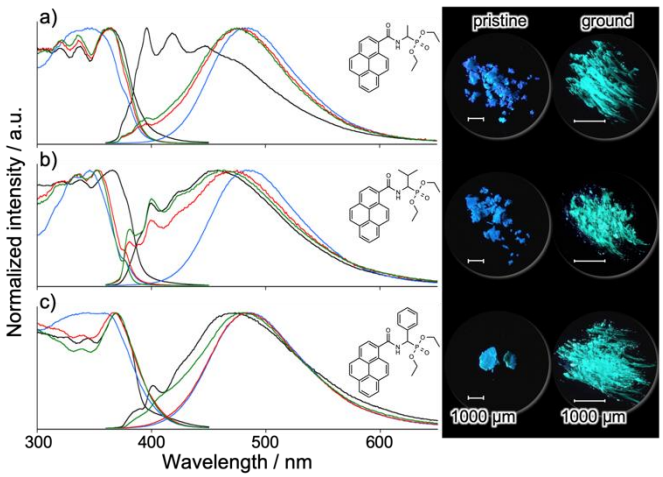

Figure 3. Excitation/emission spectra of a) **AP1**, b) **AP2** and c) **AP3** (black line: pristine, blue line: ground, red line: 30 min at RT after grinding, green line: 30 min at RT and 30 min heating at 50˚C after grinding, λ_{ex} = 340 nm, λ_{obs} = 480 nm, in solid state), and corresponding pictures under microscope with UV irradiation (λ_{ex} = 365 nm).

The pristine solid-state samples exhibited blue fluorescence with narrow bands in shorter (390-430nm) wavelengths and broader bands in longer (430-600nm) wavelengths (Figure 3, black line). Since the emission peaks in solid state partially overlapped with those in solution (385-405 nm), the monomer contribution is expected in the shorter wavelength region. The different intensity ratio of narrow/broad emission bands (**AP1** > **AP2** > **AP3**) would be due to the characteristic packing motifs with different significance of face-to-face contacts: **AP1** shows the weakest intermolecular interactions whereas **AP3** displays both short π-π distances and long-range columnar stacking. Upon grinding with a pestle in a mortar, blue-to-green fluorescence colour change was clearly observed. In order to take into account not only the maximum emission wavelength change but also the spectral broadening or narrowing upon grinding, the fluorescence colour change was estimated using the mean wavelength shift $\Delta\lambda$ with λ_{mean} defined by equation 1:

$$\boldsymbol{\lambda_{mean}} = \frac{\int_0^\infty \lambda \times I_F(\lambda)\, d\lambda}{\int_0^\infty I_F(\lambda)\, d\lambda}, \quad (1)$$

where $I_F(\lambda)$ is the intensity of the emission spectra. The estimated λ_{mean} values are summarized in Table 1. The largest MFC shift was estimated for **AP1** ($\Delta\lambda_{AP1}$ = 40 nm, $\Delta\nu_{AP1}$ = −1700 cm^{-1}), followed by **AP2** ($\Delta\lambda_{AP2}$ = 29 nm, $\Delta\nu_{AP2}$ = −1200 cm^{-1}) and **AP3** ($\Delta\lambda_{AP3}$ = 10 nm, $\Delta\nu_{AP3}$ = −400 cm^{-1}). After grinding the recorded spectral profiles were quite similar among these three compounds with a single broad structureless band centred at around 500 nm (Figure 3, blue line), and the narrow peaks in shorter wavelength were not observed. We also realized that the green fluorescence of **AP2** immediately started turning back to the original blue fluorescence. Back reaction without solvent fuming or thermal annealing has been observed on different types of mechanofluorochromic compounds[21-25] however the molecular design leading to this spontaneous reversibility is still poorly understood. Therefore, we considered the solid-state structural change including back reaction, and spectra of ground samples of **AP1-3** were taken at different time intervals after grinding (see Figure 3, red lines for 30min at RT after grinding).

Table 1. Sample state and corresponding emission mean wavelength.

Sample state[a]	AP1	AP2	AP3
Pristine / nm	459	472	491
Ground / nm	499	501	501
10 min at RT / nm	492	491	501
20 min at RT / nm	489	480	501
30 min at RT / nm	488	478	501
30 min at RT + 30 min at 50˚C / nm	484	473	493
Total shift at RT[b] / nm	40	29	10

[a] All samples were treated at room temperature. [b] Total shift = $\lambda_{mean,ground} - \lambda_{mean,pristine}$.

It is interesting to mention that all of these compounds show different thermal back reaction behaviours. For each compound, the λ_{mean} values were plotted against time after grinding, and the resulting data were fitted with a mono-exponential decay (Figure S2). At room temperature, **AP3** appears almost bistable, while the two other compounds display fast relaxation processes with characteristic times between 7.9 min (**AP1**) and 12.9 minutes (**AP2**).[26, 27] However, only the exponential-decay curve for **AP2** was found to approach to the λ_{mean} of pristine form (y_0 = 487, 474 and 500 nm for **AP1**, **AP2** and **AP3**, respectively, see supporting information Figure S2). The emission mean wavelength of **AP1** indicated a rather limited back reaction in 30 min at room temperature (28% calculated as ($\lambda_{mean,ground} - \lambda_{mean,30min}$)/($\lambda_{mean,ground} - \lambda_{mean,pristine}$)) compared to that of **AP2** (81%), which suggests the existence of a second, slower kinetic constant for the back reaction, as already observed on boron-diketonate complexes.[26] Another 30 min of heating at 50˚C triggered the back reaction of **AP3**: the estimated λ_{mean} value corresponds to 84% of the complete thermal back reaction for **AP3**. This suggests that the energy barrier for the back reaction (ΔE) is smaller for **AP2** than for **AP3**. On the contrary, the back reaction of **AP1** is only slightly accelerated by heating at 50°C. Therefore, the alkyl and phenyl side groups can affect the degree of flexibility and molecular motions necessary to rearrange the intermolecular structures and form the most preferable arrangement in solid state. A rigid substituent such as phenyl has less possibility to contribute to the back reaction, while the flexible and bulky alkyl groups are more likely to favour spontaneous rearrangement of the molecular packing. The partial C-C rotation of *i*-Pr group was reported to induce solid-state phase transition caused by the synergetic changes in molecular conformation and intermolecular packing even at 200 K.[28] The stronger Ph-Ph interactions are also known to induce the higher activation energy of Ph group rotation,[29] which would be correlated with the characteristic solid-state back reaction of **AP3** at higher temperature. To confirm these assumptions, comparative thermal or structural experimental data (differential scanning calorimetry, powder X-Ray diffraction), before and after grinding, would be useful.

However, the relatively fast thermal back reaction after grinding (*vide supra*) prevent the feasibility of such measurements.

For further investigation, solid-state time-resolved fluorescence measurements of **AP1-3** were performed before and after grinding at three distinct emission wavelengths (Figure 4 and Figure S3 in supporting information). Since each fluorescence decay measurement takes several minutes, it is reasonable to think that the detected signals are not from pure ground forms. Global analysis was successfully converged for every set of three decays of each sample in the pristine or ground forms. The decay-times, their corresponding pre-exponential factors and fractions of intensity are summarized in Table 2 (see supporting information Table S3 for complete set of data). Despite more sophisticated models exist, such as distributions of decay times which may well reflect the wide variety of molecular species and packings in the solid state,[30] we decided to select a sum of three or four discrete exponentials to fit our decay curves. Indeed, this simplified and robust model led to satisfactory fits (global $\chi_R^2 < 1.2$) and turned out to be sufficient to extract useful information regarding the basic excited-state kinetics of **AP1-3**.

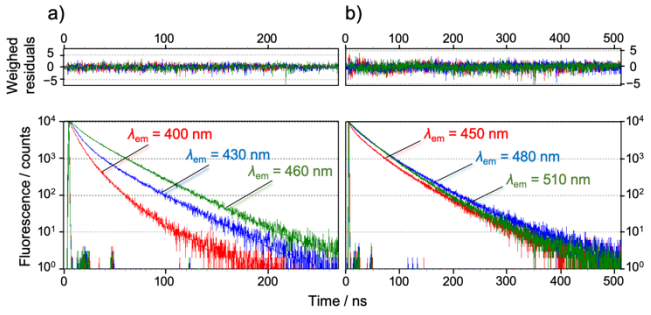

Figure 4. Fluorescence decay curves of **AP1** a) before grinding and b) after grinding recorded in solid state with weighted residuals (top) and multiexponential fitting (bottom).

Before grinding, four discrete exponentials were necessary to model the fluorescence decays for all pristine forms of **AP1-3** (Table 2). The shortest component τ_4 (0.48-1.1 ns) represents a small contribution, but shows a negative pre-exponential factor at longer emission wavelength (430-480 nm, see Table 2 and supporting information, Table S3). The fraction of intensity of the longest decay time τ_1 (>25 ns) increases in the longer emission wavelength. Such behaviour is typical of excimer emission with short rise times and long decay times in the red part of the emission spectrum. On the other hand, two intermediate time constants τ_2 and τ_3 (in the range of 2-21 ns) are identified, which represents most of the emission intensity in the blue side of the emission spectrum ($f_2 + f_3$ = 0.93, 0.79 and 0.66 at 400 nm for **AP1** and **AP2** and at 420 nm for **AP3**, respectively). It well corresponds to the structured monomer-like emission of the fluorescence spectrum (see Figure 3). Co-existence of monomer and dynamic excimer features in all pristine samples is certainly due to the specific geometrical packing of the pyrene molecules, with enhanced interactions in the excited state, allowing both emissions to arise.

Besides, the ground samples **AP1-3** were analyzed with only three components. The shortest component τ_4 (0.48-1.1 ns) observed in pristine samples as a rise time is not present any more in ground samples. Instead, a much longer decay time τ_1 (46-62 ns) appears with a high fraction of intensity (f_1 = 0.42, 0.56 and 0.61 at 480 nm for **AP1**, **AP2** and **AP3**, respectively). The novel long component, typical of the ground form, could come from a new excimer species, for which no rise time is detected. In these ground samples, preformed excimers (*i.e.* two pyrene molecules packed in a much favourable configuration) may exist, with a much shorter time of formation in the excited state than the time resolution of our instrumentation. Additionally, two other components τ_2 (22-32 ns) and τ_3 (4.2-7.0 ns) are present, which probably correspond to the dynamic excimer and monomer emissive species as identified in pristine forms. It is worth noting that the monomer component (τ_3) is associated to very low fractions of intensity ($f_3 < 0.1$ for all compounds), which is well-consistent with the complete disappearance of the structured blue emission in the steady-state spectra of **AP1-3** after grinding (Figure 3).

Table 2. Emission lifetimes τ, corresponding normalized pre-exponential factors a and fraction of intensity f of **AP1-3**[a] (λ_{ex} = 360 nm, λ_{em} = 430 nm for pristine **AP1** and **AP2**, 450 nm for pristine **AP3**, λ_{em} = 480 nm for ground form).

	τ_1 (a_1, f_1)	τ_2 (a_2, f_2)	τ_3 (a_3, f_3)	τ_4 (a_4, f_4)
AP1 pristine	31 (0.15, 0.40)	15 (0.24, 0.29)	6.0 (0.61, 0.31)	1.0 (−0.25, −0.02)
AP1 ground	62 (0.23, 0.42)	32 (0.58, 0.54)	7.0 (0.18, 0.04)	-
AP2 pristine	44 (0.11, 0.33)	21 (0.33, 0.47)	5.3 (0.56, 0.20)	1.1 (−0.02, 0.00)
AP2 ground	50 (0.36, 0.56)	26 (0.52, 0.42)	5.2 (0.12, 0.02)	-
AP3 pristine	25 (0.11, 0.53)	7.0 (0.11, 0.16)	2.0 (0.78, 0.31)	0.48 (−0.97, −0.09)
AP3 ground	46 (0.39, 0.61)	22 (0.49, 0.37)	4.2 (0.13, 0.02)	-

[a] Pre-exponential factors and fractions of intensity were normalized by the sum of positive components.

Overall, both steady-state and time-resolved fluorescence studies support the hypothesis of monomer and excimer emissive species. In pristine samples, both blue-structured and broad red fluorescence bands are typical of monomer vs. excimer emission (dynamic excimers, *cf* decay curves). In ground samples, even more red-shifted broad emission appears which is compatible with another emissive species including long-lived preformed excimers. In all cases, excitation spectra (Figure 3) neither extend over 420 nm nor being red-shifted upon grinding (even slight blue-shift is identified in the case of **AP1**). This observation corroborates the existence of excimer species in pristine and ground forms, rather than

dimer aggregates. Moreover, due to the close vicinity of molecules in the solid state and the variety of local intermolecular configurations, one cannot exclude additional processes to take place, such as energy transfer between higher energy monomers that cannot form excimers and more stabilized monomers that prone to yield excimers, which may increase the excimer-to-monomer ratio.

According to the reported crystal structure with hydrogen-substituted amidophosphonate (denoted "**AP-H**" hereafter), π-aromatic surface of pyrene moiety contributed to form face-to-face π-π stacking.[20] The MFC property of **AP-H** (Figure S4 in supporting information) indicated that the grinding process gave change in the intermolecular interactions for this molecule as well and larger MFC shift would be achieved in compounds with smaller substituents, probably due to the effect of free volume to the stacking structures.

Conclusions

In conclusion, we demonstrated the MFC properties of pyrene-derived amidophosphonates with methyl, isopropyl and phenyl side groups. The corresponding pristine crystal structures showed a variable degree of π-π and CH- π interactions depending on the substituents. The prepared compounds exhibited blue to green fluorescence colour change upon grinding. We also observed the solid-state back reaction at room temperature, which indicates that the designed steric structures can give reversible MFC system without organic solvent. Interesting monomer- and excimer-like (dynamic or preformed excimers) fluorescence features have been highlighted at the origin of the large fluorescence changes upon grinding: the molecular packing being affected by the mechanical stress, the monomer emission disappears in favour to excimer emission, associated with longer lifetimes and emission at longer wavelengths. The versatility of pyrene derivatives opens up the possibility of developing a new library of organic MFC-active compounds, and further exploration of these series would be useful to resolve the mechanism of MFC in terms of photophysics and crystallography, as well as applications for stress-sensitive materials.

Experimental

Compounds **AP1-3** were prepared and purified according to the earlier published procedure.[20]

Optical Measurements: Emission and excitation spectra of pristine powder samples were recorded on a HORIBA Jobin-Yvon Fluorolog FL3-221 spectrometer using a short path length optical quartz cell (20/C/Q/0.2, Starna), and the spectra were corrected for the response of the detector system. The pristine powder was ground using an agate mortar, and the resulting amorphous solid adhered on a pestle surface was immediately transferred to a quartz plate to record the spectra and minimize the effect of back reaction at room temperature. Fluorescence decay profiles were obtained by time-correlated single-photon counting (TCSPC) method with titanium:sapphire laser (Tsunami, Spectra-Physics) pumped by a doubled Nd:YVO_4 laser (Millennia Xs, Spectra-Physics). Light pulses at 780 nm, for solution samples (resp. 740 nm for powder samples), were selected by an acousto-optic crystal at a repetition rate of 0.8 MHz, and then doubled at 390 nm (resp. 370 nm) by nonlinear crystals. Fluorescence photons were detected at 90˚ through a polarizer at the magic angle and monochromator, by means of a Hamamatsu MCP R3809U photomultiplier, connected to a SPC-630 TCSPC module from Becker&Hickl. The instrumental response function was recorded before each decay measurement with a fwhm (full width half maximum) of 860 ps. The fluorescence data were analyzed using the Globals software package developed at the Laboratory for Fluorescence Dynamics at the University of Illinois at Urbana-Champaign, which includes reconvolution analysis and global non-linear least-squares minimization method.

Photography: Pictures before/after grinding were taken by KEYENCE free-angle observation system base unit VHX-S550E with stereomicroscope fluorescence adapter (λ_{ex} = 365 nm).

Crystallography: The measurements were performed on a VENTURE PHOTON100 CMOS Bruker diffractometer with Micro-focus IuS source Cu Kα radiation. Crystals were mounted on a CryoLoop with Paratone-N (Hampton Research) as cryoprotectant and then flashfrozen in a nitrogen-gas stream at 100 K. For compounds, the temperature of the crystal was maintained at the selected value by means of a 700 series Cryostream cooling device to within an accuracy of ±1 K. The data were corrected for Lorentz polarization, and absorption effects. The structures were solved by direct methods using SHELXS-97[31] and refined against F^2 by full-matrix least-squares techniques using SHELXL-2018[32] with anisotropic displacement parameters for all non-hydrogen atoms. Hydrogen atoms were located on a difference Fourier map and introduced into the calculations as a riding model with isotropic thermal parameters. All calculations were performed by using the Crystal Structure crystallographic software package WINGX.[33] The crystal data collection and refinement parameters are given in Table S1. CCDC 1973249 (**AP1**); 1973250 (**AP2**) and 1973251 (**AP3**) contains the supplementary crystallographic data for this paper. These data can be obtained free of charge from the Cambridge Crystallographic Data Centre via http://www.ccdc.cam.ac.uk/Community/Requestastructure.

Conflicts of interest

There are no conflicts to declare.

Acknowledgements

Y. H. gratefully acknowledges support from the Japan Society of the Promotion of Science (JSPS). R.M. and C. A. acknowledge ERC funding 'MECHANOFLUO' (St-G 715757) project.

References

1. Y. Sagara, S. Yamane, M. Mitani, C. Weder and T. Kato, *Adv. Mater.*, 2016, **28**, 1073-1095.
2. B.-H. Di and Y.-L. Chen, *Chin. Chem. Lett.*, 2018, **29**, 245-251.
3. Z. Chi, X. Zhang, B. Xu, X. Zhou, C. Ma, Y. Zhang, S. Liu and J. Xu, *Chem. Soc. Rev.*, 2012, **41**, 3878-3896.
4. P. Xue, J. Ding, P. Wang and R. Lu, *J. Mater. Chem. C*, 2016, **4**, 6688-6706.
5. C. Calvino, L. Neumann, C. Weder and S. Schrettl, *J. Polym. Sci., Part A: Polym. Chem.*, 2017, **55**, 640-652.
6. G. Zhang, J. Lu, M. Sabat and C. L. Fraser, *J. Am. Chem. Soc.*, 2010, **132**, 2160-2162.
7. L. Wilbraham, M. Louis, D. Alberga, A. Brosseau, R. Guillot, F. Ito, F. Labat, R. Metivier, C. Allain and I. Ciofini, *Adv Mater*, 2018, **30**, e1800817.
8. H. Ito, M. Muromoto, S. Kurenuma, S. Ishizaka, N. Kitamura, H. Sato and T. Seki, *Nat. Commun.*, 2013, **4**, 2009.
9. T. Seki, Y. Takamatsu and H. Ito, *J. Am. Chem. Soc.*, 2016, **138**, 6252-6260.
10. A. Wrona-Piotrowicz, J. Zakrzewski, R. Métivier, A. Brosseau, A. Makal and K. Woźniak, *RSC Adv.*, 2014, **4**, 56003-56012.
11. Y. Niko, Y. Cho, S. Kawauchi and G.-i. Konishi, *RSC Adv.*, 2014, **4**.
12. J. Hwang, M. G. Choi, S. Eor and S. K. Chang, *Inorg. Chem.*, 2012, **51**, 1634-1639.
13. X. Feng, J. Y. Hu, C. Redshaw and T. Yamato, *Chem. Eur. J.*, 2016, **22**, 11898-11916.
14. S. K. Rajagopal, A. M. Philip, K. Nagarajan and M. Hariharan, *Chem. Commun.*, 2014, **50**, 8644-8647.
15. Y. Sagara, T. Mutai, I. Yoshikawa and K. Araki, *J. Am. Chem. Soc.*, 2007, **129**, 1520-1521.
16. E. Nagata, S. Takeuchi, T. Nakanishi, Y. Hasegawa, Y. Mawatari and H. Nakano, *ChemPhysChem*, 2015, **16**, 3038-3043.
17. V. C. Wakchaure, K. C. Ranjeesh, Goudappagouda, T. Das, K. Vanka, R. Gonnade and S. S. Babu, *Chem. Commun.*, 2018, **54**, 6028-6031.
18. G. Li, Y. Xu, W. Zhuang and Y. Wang, *RSC Adv.*, 2016, **6**, 84787-84793.
19. Y. Sagara, T. Komatsu, T. Ueno, K. Hanaoka, T. Kato and T. Nagano, *Adv. Funct. Mater.*, 2013, **23**, 5277-5284.
20. A. Wrona-Piotrowicz, J. Zakrzewski, A. Gajda, T. Gajda, A. Makal, A. Brosseau and R. Metivier, *Beilstein J. Org. Chem.*, 2015, **11**, 2451-2458.
21. D. Tu, P. Leong, Z. Li, R. Hu, C. Shi, K. Y. Zhang, H. Yan and Q. Zhao, *Chem. Commun.*, 2016, **52**, 12494-12497.
22. F. Zhao, C. Fan, Z. Chen, G. Liu and S. Pu, *RSC Adv.*, 2017, **7**, 43845-43848.
23. S. Ito, T. Taguchi, T. Yamada, T. Ubukata, Y. Yamaguchi and M. Asami, *RSC Adv.*, 2017, **7**, 16953-16962.
24. K. Mizuguchi, H. Kageyama and H. Nakano, *Mater. Lett.*, 2011, **65**, 2658-2661.
25. T. Butler, W. A. Morris, J. Samonina-Kosicka and C. L. Fraser, *ACS Appl. Mater. Interfaces*, 2016, **8**, 1242-1251.
26. T. Sagawa, F. Ito, A. Sakai, Y. Ogata, K. Tanaka and H. Ikeda, *Photochem. Photobiol. Sci.*, 2016, **15**, 420-430.
27. M. Louis, A. Brosseau, R. Guillot, F. Ito, C. Allain and R. Métivier, *J. Phys. Chem. C*, 2017, **121**, 15897-15907.
28. U. D. Pete, A. G. Dikundwar, V. M. Sharma, S. P. Gejji, R. S. Bendre and T. N. Guru Row, *CrystEngComm*, 2015, **17**, 7482-7485.
29. P. C. Hägele and L. Beck, *Macromolecules*, 1977, **10**, 213-215.
30. R. Métivier, I. Leray, M. Roy-Auberger, N. Zanier-Szydlowski and B. Valeur, *New J. Chem.*, 2002, **26**, 411-415.
31. G. M. Sheldrick, *SHELXS-97, Program for Crystal Structure Solution*, University of Göttingen, Göttingen, Germany, 1997
32. G. M. Sheldrick, *Acta Crystallogr., Sect. A: Found. Crystallogr.*, 2008, **64**, 112-122.
33. L. J. Farrugia, *J. Appl. Cryst.*, 1999, **32**, 837.